

Photon pair-state preparation with tailored spectral properties by spontaneous four-wave mixing in photonic-crystal fiber

K. Garay-Palmett,^{1*} H. J. McGuinness,² Offir Cohen,³ J. S. Lundeen,³
R. Rangel-Rojo,¹ A. B. U'Ren,¹ M. G. Raymer,² C. J. McKinstrie,⁴
S. Radic,⁵ and I. A. Walmsley³

¹ *Departamento de Optica, Centro de Investigación Científica y de Educación Superior de Ensenada, Apartado Postal 2732, Ensenada, BC 22860, Mexico.*

² *Department of Physics, University of Oregon, Eugene, OR 97403, United States.*

³ *Clarendon Laboratory, Oxford University, Parks Road, Oxford, OX1 3PU, United Kingdom*

⁴ *Bell Laboratories, Alcatel-Lucent, Holmdel, NJ 07733, United States.*

⁵ *Department of Electrical and Computer Engineering, University of California at San Diego, La Jolla, CA 92093, United States.*

*corresponding author: kgaray@cicese.mx

Abstract: We study theoretically the generation of photon pairs by spontaneous four-wave mixing (SFWM) in photonic crystal optical fiber. We show that it is possible to engineer two-photon states with specific spectral correlation (“entanglement”) properties suitable for quantum information processing applications. We focus on the case exhibiting no spectral correlations in the two-photon component of the state, which we call factorability, and which allows heralding of single-photon pure-state wave packets without the need for spectral post filtering. We show that spontaneous four wave mixing exhibits a remarkable flexibility, permitting a wider class of two-photon states, including ultra-broadband, highly-anticorrelated states.

© 2018 Optical Society of America

OCIS codes: (190.4380)Nonlinear optics, four-wave mixing; (270.0270) Quantum optics.

References and links

1. See, for example, the review by P. Kok, W. J. Munro, K. Nemoto, T. C. Ralph, J. P. Dowling and G. J. Milburn, “Linear optical quantum computing with photonic qubits,” *Rev. Mod. Phys.* **79**, 135–174 (2007).
2. S. E. Harris, M. K. Oshman, and R. L. Byer, “Observation of Tunable Optical Parametric Fluorescence,” *Phys. Rev. Lett.* **18**, 732–734 (1967).
3. A. B. U'Ren, C. Silberhorn, K. Banaszek, I. A. Walmsley, R. Erdmann, W. P. Grice and M. G. Raymer, “Generation of pure-state single-photon wavepackets by conditional preparation based on spontaneous parametric downconversion,” *Laser Phys.* **15**, 146–161 (2005).
4. M. G. Raymer, J. Noh, K. Banaszek and I. A. Walmsley, “Pure-state single-photon wave-packet generation by parametric down-conversion in a distributed microcavity,” *Phys. Rev. A* **72**, 023825 (2005).
5. A. B. U'Ren, C. Silberhorn, K. Banaszek and I.A. Walmsley, “Efficient conditional preparation of high-fidelity single photon states for fiber-optic quantum networks,” *Phys. Rev. Lett.* **93**, 093601 (2004).
6. K. Banaszek, A. B. U'Ren and I. A. Walmsley, “Generation of correlated photons in controlled spatial modes by downconversion in nonlinear waveguides,” *Opt. Lett.* **26**, 1367–1369 (2001).
7. J. Fan and A. Migdall, “A broadband high spectral brightness fiber-based two-photon source,” *Opt. Express* **15**, 2915–2920 (2007).

8. J. Rarity, J. Fulconis, J. Duligall, W. Wadsworth, and P. St. J. Russell, "Photonic crystal fiber source of correlated photon pairs," *Opt. Express* **13**, 534–544 (2005).
9. J. Fan and A. Migdall, "Generation of cross-polarized photon pairs in a microstructure fiber with frequency-conjugate laser pump pulses," *Opt. Express* **13**, 5777–5782 (2005).
10. X. Li, J. Chen, P. Voss, J. Sharping, and P. Kumar, "All-fiber photon-pair source for quantum communications: Improved generation of correlated photons," *Opt. Express* **12**, 3737–3744 (2004).
11. W. P. Grice, A. B. U'Ren and I. A. Walmsley, "Eliminating frequency and space-time correlations in multiphoton states," *Phys. Rev. A* **64**, 063815 (2001).
12. P. Russell, "Photonic Crystal Fiber," *Science* **299**, 358–362 (2003).
13. M. Fiorentino, P. L. Voss, J. E. Sharping and P. Kumar, "All-fiber photon-pair source for quantum communications," *IEEE Photon. Technol. Lett.* **14**, 983–985 (2002).
14. R. H. Stolen, "Fundamentals of Raman amplification in fibers," in *Raman Amplifiers for Telecommunications 1*, edited by M. N. Islam (Springer, 2003), pp. 35–59.
15. R. Jiang, R. Saperstein, N. Alic, M. Nezhad, C. J. McKinstrie, J. Ford, S. Fainman and S. Radic, "Parametric wavelength conversion from conventional near-infrared to visible band," *IEEE Photon. Technol. Lett.* **18**, 2445–2447 (2006).
16. J. D. Harvey, R. Leonhardt, S. Coen, G. K. L. Wong, J. C. Knight, W. J. Wadsworth and P. St. J. Russell, "Scalar modulation instability in the normal dispersion regime by use of a photonic crystal fiber," *Opt. Lett.* **28**, 2225–2227 (2003).
17. M. Yu, C. J. McKinstrie and G. P. Agrawal, "Modulational instabilities in dispersion-flattened fibers," *Phys. Rev. E* **52**, 1072–1080 (1995).
18. Peter J. Mosley, Jeff S. Lundeen, Brian J. Smith, Ian A. Walmsley, Piotr Wasylczyk, Alfred B. U'Ren, Christine Silberhorn, in *Coherence and Quantum Optics IX*, (Kluwer Academic/Plenum, New York) (accepted).
19. Z.D. Walton, A. V. Sergienko, B. E. A. Saleh, and M. C. Teich, "Polarization-Entangled Photon Pairs with Arbitrary Joint Spectrum" *Phys. Rev. A* **70**, 052317 (2004)
20. J. P. Torres, F. Macia, S. Carrasco, and L. Torner, "Engineering the frequency correlations of entangled two-photon states by achromatic phase matching" *Opt. Lett.* **30**, 314 (2005)
21. O. Kuzucu, M. Fiorentino, M. A. Albota, F. N. C. Wong, and F. X. Kärtner, *Phys. Rev. Lett.* **94**, 083601 (2005)
22. A. B. U'Ren, K. Banaszek and I. A. Walmsley, "Photon engineering for quantum information processing" *Quantum Information and Computation* **3**, 480 (2003)
23. A. B. U'Ren, R. Erdmann, M. De la Cruz and I. A. Walmsley, "Generation of two-photon states with an arbitrary degree of entanglement via nonlinear crystal superlattices," *Phys. Rev. Lett.* **97**, 223602 (2006).
24. V. Giovanetti, S. Lloyd and L. Maccone, "Quantum-enhanced positioning and clock synchronization," *Nature* **412**, 417–419 (2001).
25. M. B. Nasr, B. E. A. Saleh, A. V. Sergienko and M. C. Teich, "Demonstration of dispersion-canceled quantum-optical coherence tomography," *Phys. Rev. Lett.* **91**, 083601 (2003).
26. L. Mandel and E. Wolf, *Optical Coherence and Quantum Optics* (Cambridge University Press, 1995).
27. J. Chen, X. Li and P. Kumar, "Two-photon-state generation via four-wave mixing in optical fibers," *Phys. Rev. A* **72**, 033801 (2005).
28. J. Chen, K. F. Lee and P. Kumar R, "Quantum theory of degenerate $\chi^{(3)}$ two-photon state," e-print arXiv:quant-ph/0702176v1.
29. G. P. Agrawal, *Nonlinear Fiber Optics, 4th Ed.* (Elsevier, 2007).
30. C. J. McKinstrie, H. Kogelnik and L. Schenato, "Four-wave mixing in a rapidly-spun fiber," *Opt. Express* **15**, 8516–8534 (2006). This paper also reviews scalar and vector FWM in strongly-birefringent and randomly-birefringent fibers.
31. K. P. Hansen, "Dispersion flattened hybrid-core nonlinear photonic crystal fiber," *Opt. Express* **11**, 1503–1509 (2003).
32. T. A. Birks, J. C. Knight and P. St. J. Russell. "Endlessly single-mode photonic crystal fiber," *Opt. Lett.* **22**, 961–963 (1997).
33. G. K. L. Wong, A. Y. H. Chen, S. W. Ha, R. J. Kruhlak, S. G. Murdoch, R. Leonhardt, J. D. Harvey and N. Y. Joly, "Characterization of chromatic dispersion in photonic crystal fibers using scalar modulation instability," *Opt. Express* **13**, 8662–8670 (2005).
34. A. Ortigosa-Blanch, A. Diez, M. Delgado-Pinar, J. L. Cruz and Miguel V. Andres, "Ultrahigh birefringent nonlinear microstructured fiber," *IEEE Photon. Technol. Lett.* **16**, 1667–1669 (2004).
35. A. L. Berkhoer and V. E. Zakharov, "Self-excitation of waves with different polarizations in nonlinear media," *Sov. Phys. JETP* **31**, 486–493 (1970).
36. C. J. McKinstrie and S. Radic, "Phase-sensitive amplification in a fiber," *Opt. Express* **12**, 4973–4979 (2004).
37. R. H. Stolen, M. A. Bosch and C. Lin, "Phase matching in birefringent fibers," *Opt. Lett.* **6**, 213–215 (1981).
38. R. J. Kruhlak, G. K. L. Wong, J. S. Y. Chen, S. G. Murdoch, R. Leonhardt, J. D. Harvey, N. Y. Joly and J. C. Knight, "Polarization modulation instability in photonic crystal fibers," *Opt. Lett.* **31**, 1379–1381 (2006).
39. S. G. Murdoch, R. Leonhardt and J. D. Harvey, "Polarization modulation instability in weakly birefringent fibers," *Opt. Lett.* **20**, 866–868 (1995).

40. Q. Lin, F. Yaman and G. P. Agrawal, "Photon-pair generation by four-wave mixing in optical fibers," *Opt. Lett.* **31**, 1286–1288 (2006).
 41. Q. Lin, F. Yaman and G. P. Agrawal, "Photon-pair generation in optical fibers through four-wave mixing: Role of Raman scattering and pump polarization," *Phys. Rev. A* **75**, 023803 (2007).
 42. Such a state is typically referred to as highly entangled, but one should keep in mind that the large vacuum component of the state renders this "entanglement" useful only in a post-selection experiment.
 43. K. A. O'Donnell and A. B. U'Ren, "Observation of ultrabroadband, beamlike parametric downconversion," *Opt. Lett.* **32**, 817–819 (2007).
 44. L. Zhang, A. B. U'Ren, R. Erdmann, K. A. O'Donnell, C. Silberhorn, K. Banaszek and I. A. Walmsley, "Generation of highly entangled photon pairs for continuous variable Bell inequality violation," *J. Mod. Opt.* **54**, 707–719 (2007).
 45. R. Jiang, N. Alic, C. J. McKinstrie and S. Radic, "Two-pump parametric amplifier with 40 dB of equalized gain over a bandwidth of 50 nm," *Proc. OFC 2007*, paper OWB2.
 46. J. M. Chavez Boggio, J. D. Marconi, S. R. Bickham and H. L. Fragnito, "Spectrally flat and broadband double-pumped fiber optical parametric amplifiers," *Opt. Express* **15**, 5288–5309 (2007).
 47. S. Radic, C. J. McKinstrie, R. M. Jopson, J. C. Centanni, Q. Lin and G. P. Agrawal, "Record performance of parametric amplifier constructed with highly nonlinear fibre," *Electron. Lett.* **39**, 838–839 (2003).
 48. H. Takesue and K. Inoue, "1.5- μm band quantum-correlated photon pair generation in dispersion-shifted fiber: suppression of noise photons by cooling fiber," *Opt. Express* **13**, 7832–7839 (2005).
-

1. Introduction

Quantum optical technologies require photon states with specific spectral properties. For example, quantum information processing using linear optics is based upon the availability of pure-state single-photon wavepackets [1]. Single-photon wavepackets can be prepared using pair generation by means of spontaneous parametric downconversion (PDC), or by spontaneous four wave mixing (SFWM) [2]. In both cases individual photons are heralded by the detection of their siblings. The prepared photons will not normally be in pure states unless special care is taken to remove all correlations in every degree of freedom of the photon pairs, i.e. to make the two-photon state factorable[3]. If this is not done, the heralded photons will be in mixed states, and therefore unsuitable for use in quantum logic gates, which rely on Hong-Ou-Mandel (HOM) interference between independent photons. Typically, photon pairs generated in spontaneous processes exhibit significant spectral and spatial correlations due to the energy and momentum conservation constraints that are typical in parametric nonlinear optics. Spatial correlations may be minimized by use of guided-wave configurations, such as those exploiting nonlinear waveguides and optical fibers[4, 5, 6, 7, 8, 9, 10].

Spectral correlations are, however, more difficult to eliminate. It is possible to eliminate all correlations in this degree of freedom for photon pairs generated by means of PDC, as first shown in Ref. [11], and later extended in [3]. This is achieved by the method of group-velocity matching using a broadband pump pulse. In this paper we generalize this method to the case of SFWM, by engineering the group velocities of the sideband photons using photonic crystal fibers (PCFs). PCFs are comprised of a solid silica core surrounded by a silica cladding containing a regular array of air holes. This leads to an exceptionally high core-cladding index contrast, creating strong waveguide dispersion that can be tailored for a wide-range of applications [12].

Spontaneous four wave mixing occurs in single-mode fibers with a third-order optical nonlinearity. In this process, two pump photons are scattered from one or two distinct pump fields into a pair of fields, labeled signal and idler, which are spectrally and/or polarization distinct. The single-mode waveguide geometry leads to the suppression of correlations in the transverse momentum degree of freedom, as well as suppression of mixed spectral-transverse momentum correlations. Thus, by imposing appropriate group velocity matching constraints on the SFWM process in a single-mode fiber, it becomes possible to eliminate correlations in *all* degrees of freedom, resulting in factorable two-photon states.

Previous experimental work has explored this type of source in a number of geometries

including standard single-mode fiber and PCF. Photon number correlations between signal and idler fields were first observed by pumping in the anomalous dispersion region [13], although there was a significant background of noise photons generated by Raman scattering of the pump light [14]. Spontaneous Raman scattering generates photons shifted to the red of the pump wavelength by up to 50 THz, corresponding to the frequency of an optical phonon in glass. Thermal population of the phonons gives rise to scattering over a broad frequency range, and the process does not require phase matching, so it occurs at all pump wavelengths. Photonic crystal fibers allow the signal and idler fields to be widely separated in frequency from the pump, so that Raman noise at the lower-frequency photon wavelength is greatly reduced [7, 8]. Phase-matching of SFWM with widely separated sidebands is enabled by pumping in the normal dispersion region, which requires the favorable dispersion properties of strongly guided waves [15, 16, 17].

These experiments did not, however, address the requirement of purity for generating heralded single-photon states. In particular, the photons generated in those experiments would require tight spectral filtering to eliminate correlations between signal and idler frequencies prior to heralding. Using such tight filtering ensures high-visibility HOM interference between photons from separate sources, but greatly reduces the count rates. To avoid the need for filtering, the SFWM process must produce a state whose two-photon component can be written as the product of the signal state and the idler state, i.e., $|\psi\rangle = |0\rangle_s|0\rangle_i + \kappa|1\rangle_s|1\rangle_i$, in the photon number basis with s, i indicating signal and idler modes respectively. We call this property “factorability,” which corresponds to the absence of correlations between the frequencies (and momenta) of the idler and signal photons. In physical terms, factorability implies that no information about, say, the idler photon (apart from its existence) can be extracted from the detection of the signal photon, or vice-versa. To date, such factorable states have been produced only in PDC at a single wavelength using a particular crystal having special dispersion properties [18], and other techniques could in principle be used to extend possible operation wavelengths [4, 19, 20, 21, 22, 23]. We show here that factorability can be achieved at a much wider range of wavelengths by using PCF.

In addition to factorability, PCF enables the production of a wide range of spectral correlations in the two-photon component of the state. Two extremes are possible, a spectrally correlated state and a spectrally anti-correlated state. The former is a resource for quantum-enhanced quantum positioning [24], whereas the latter is of importance for applications relying on time-of-arrival differences between two optical modes, such as optical coherence tomography [25]. We will show that the anti-correlated case can be made ultra-broadband by tailoring the higher-order dispersion. Thus we see that the ability to engineer the dispersion in PCF leads to a flexible system that can generate states in two widely disparate regimes (factorable and highly correlated), and indeed in a very general class of intermediate regimes.

In all these cases, the light is produced in well-defined fiber modes, which is convenient for integration with waveguide devices. This holds the promise of combining many quantum logic gates using integrated optics, leading to the possibility of scalable quantum optical devices.

2. Spontaneous four wave mixing theory

In this paper we study SFWM in a single-mode optical fiber with a third-order nonlinear susceptibility $\chi^{(3)}$. In this process, two-photons from pump fields E_1 and E_2 are jointly annihilated to create a photon pair comprised of one photon in the signal mode, \hat{E}_s , and one photon in the idler mode \hat{E}_i . We assume that all fields propagate in the fundamental spatial mode of the fiber. This assumption is justified if the fiber core radius is small enough that it only supports the fundamental mode, or alternatively if only this fundamental mode is excited. Following a standard perturbative approach [26], the two-photon state produced by spontaneous four-wave

mixing in an optical fiber of length L can be shown to be given by [27, 28]

$$|\Psi\rangle = |0\rangle_s |0\rangle_i + \kappa \int \int d\omega_s d\omega_i F(\omega_s, \omega_i) |\omega_s\rangle_s |\omega_i\rangle_i. \quad (1)$$

Here, κ is a constant which represents the generation efficiency (linearly proportional to the fiber length, electric field amplitude for each of the pump fields and dependent on the relative polarizations of the pump and created pair fields) and $F(\omega_s, \omega_i)$ is the joint spectral amplitude function (JSA), which describes the spectral entanglement properties of the generated photon pair

$$F(\omega_s, \omega_i) = \int d\omega' \alpha_1(\omega') \alpha_2(\omega_s + \omega_i - \omega') \times \text{sinc} \left[\frac{L}{2} \Delta k(\omega', \omega_s, \omega_i) \right] \exp \left[i \frac{L}{2} \Delta k(\omega', \omega_s, \omega_i) \right], \quad (2)$$

which is given in terms of the pump spectral amplitudes $\alpha_{1,2}(\omega)$, and the phase mismatch function $\Delta k(\omega_1, \omega_s, \omega_i)$, that in the case where the two pumps, signal and idler are co-polarized, is given by

$$\Delta k(\omega_1, \omega_s, \omega_i) = k(\omega_1) + k(\omega_s + \omega_i - \omega_1) - k(\omega_s) - k(\omega_i) - (\gamma_1 P_1 + \gamma_2 P_2), \quad (3)$$

which includes a self/cross-phase modulation contribution for the two pumps with peak powers P_1 and P_2 , characterized by the nonlinear parameters γ_1 and γ_2 , which depend on specific fiber used and pump wavelength[29, 30]. The energy conservation constraint is apparent in the argument of the second term of the phase mismatch (see Eq.(3)). A ‘‘factorable’’ state is defined to be a state for which $F(\omega_s, \omega_i)$ is equal to a product of two functions, $F(\omega_s, \omega_i) = S(\omega_s)I(\omega_i)$, where the functions $S(\omega)$ and $I(\omega)$ depend only on the signal and idler frequencies respectively.

By making use of a linear approximation for the phase mismatch, in addition to modeling $\alpha_{1,2}(\omega)$ as Gaussian functions with bandwidth $\sigma_{1,2}$ respectively, it is possible to obtain an expression for the joint spectral amplitude in closed analytical form. Expanding $k(\omega_\mu)$ in a first-order Taylor series about frequencies ω_μ^0 for which perfect phase-matching is attained (where $\mu = 1, 2, s, i$), and defining the detunings $v_s = \omega_s - \omega_s^0$ and $v_i = \omega_i - \omega_i^0$, the approximate phase mismatch Δk_{lin} is defined by

$$L\Delta k_{lin} = L\Delta k^{(0)} + T_s v_s + T_i v_i, \quad (4)$$

where $\Delta k^{(0)}$, given by Eq.(3) evaluated at the frequencies ω_μ^0 , must vanish to guarantee phase-matching at these center frequencies. The coefficients T_μ are given by $T_\mu = \tau_\mu + \tau_p \sigma_1^2 / (\sigma_1^2 + \sigma_2^2)$, where τ_μ represent group-velocity mismatch terms between the pump centered at frequency ω_2^0 and the generated photon centered at the frequency ω_μ^0 , and τ_p is the group velocity mismatch between the two pumps

$$\begin{aligned} \tau_\mu &= L \left[k_2^{(1)}(\omega_2^0) - k_\mu^{(1)}(\omega_\mu^0) \right], \\ \tau_p &= L \left[k_1^{(1)}(\omega_1^0) - k_2^{(1)}(\omega_2^0) \right], \end{aligned} \quad (5)$$

written in terms of $k_\mu^{(n)}(\omega) = d^n k_\mu / d\omega^n |_{\omega=\omega_\mu^0}$. Note that this approach requires *a priori* knowledge, for given pump fields, of the signal and idler frequencies (ω_s^0 and ω_i^0) at which perfect

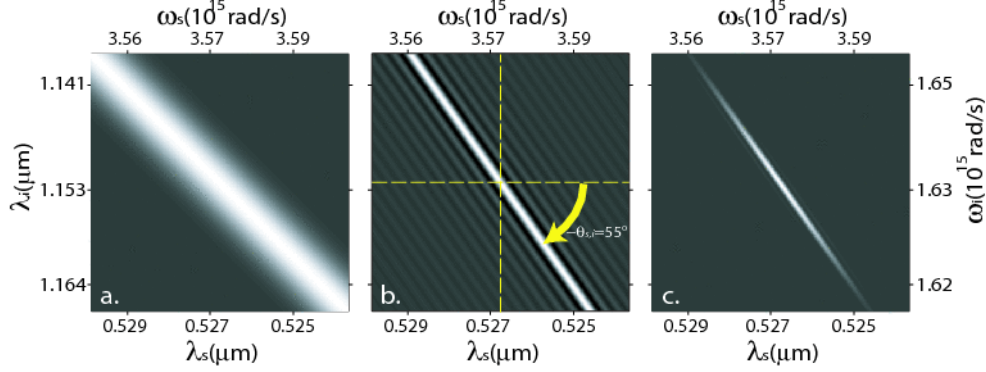


Fig. 1. (a) Pump envelope function $\alpha(\omega_s, \omega_i)$ for a fiber characterized by $r = 0.67 \mu\text{m}$, $f = 0.52$ and $L = 30\text{cm}$. (b) Phase-matching function $\phi(v_s, v_i)$; for a relatively small region of $\{\omega_s, \omega_i\}$ space the phase-matching function contours are essentially straight lines, with slope $\theta_{si} = -\arctan(T_s/T_i)$ (with T_μ given by Eq. (5)). (c) Resulting joint spectral intensity.

phase-matching is achieved. These frequencies can be determined by solving (for example numerically) the condition $\Delta k^{(0)} = 0$ (see Eq.(3)). It can be shown that within the linear approximation, the integral in Eq. (2) can be carried out analytically, yielding

$$F_{lin}(v_s, v_i) = \alpha(v_s, v_i) \phi(v_s, v_i), \quad (6)$$

where the pump envelope function $\alpha(v_s, v_i)$ is derived from the pump spectral amplitudes for the two individual pump fields through the integral in Eq. (2), and is given by

$$\alpha(v_s, v_i) = \exp\left[-\frac{(v_s + v_i)^2}{\sigma_1^2 + \sigma_2^2}\right], \quad (7)$$

and where $\phi(v_s, v_i)$ describes the phase-matching properties in the fiber. For degenerate pumps (where $\alpha_1(\omega) = \alpha_2(\omega)$), it may be shown that the phase-matching function is given by

$$\phi(v_s, v_i) = \text{sinc}\left[\frac{L\Delta k_{lin}}{2}\right] \exp\left[i\frac{L\Delta k_{lin}}{2}\right], \quad (8)$$

where $L\Delta k_{lin}$ is given in Eq. (4) with $\tau_p = 0$. For non-degenerate pumps, $\tau_p \neq 0$ and $\phi(v_s, v_i) = \Phi(B; L\Delta k_{lin})$, with

$$\Phi(B; x) = M\sqrt{\pi}B \exp(-B^2 x^2) \left[\text{erf}\left(\frac{1}{2B} - iBx\right) + \text{erf}(iBx) \right], \quad (9)$$

where $\text{erf}(z)$ is the error function, the parameter B is defined as $B = (\sigma_1^2 + \sigma_2^2)^{1/2} / (\sigma_1 \sigma_2 \tau_p)$, and M is a normalization coefficient. In the present paper, we concentrate on the important class of factorable states for which $F(\omega_s, \omega_i) = S(\omega_s)I(\omega_i)$.

3. Phase and group-velocity matching properties of photonic crystal fibers

Our analysis focuses on PCFs consisting of a fused silica core surrounded by silica cladding with a pattern of air holes which remains constant along the fiber length. This mixture of air and

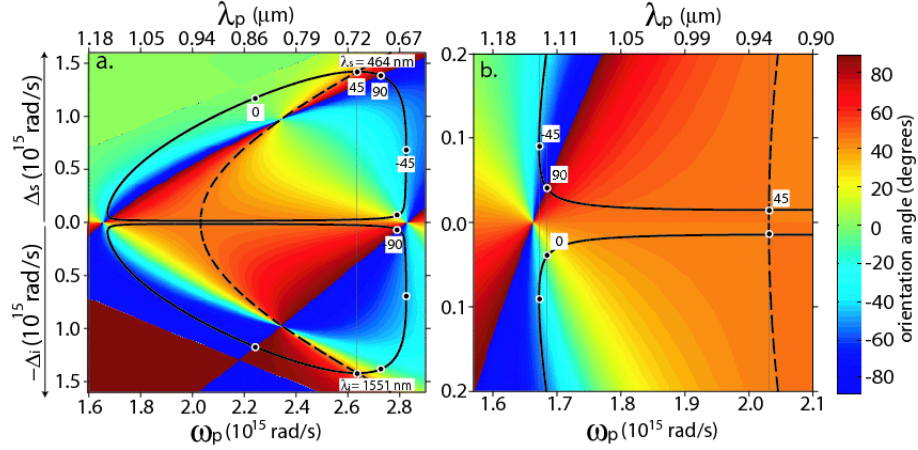


Fig. 2. (a) Black, solid curve: phase-matching ($\Delta k = 0$) contour for SFWM in the degenerate pump case. Colored background: phase-matching orientation angle. Black, dashed line: symmetric group velocity matching (GVM) contour. Along the phase-matching contour we have indicated particular orientation angles of interest. (b) Close up, near the lower zero group velocity dispersion frequency.

and glass in the cladding results in an average refractive index that is considerably lower than that of the core, providing a high dielectric contrast, resulting in strong optical confinement. This leads to high peak irradiances even for modest input powers, which enhances nonlinear optical effects such as SFWM. In addition, the dispersion characteristics of the PCFs can be engineered by variations of the distribution, size and shape of the air holes surrounding the core. In particular, it becomes possible to choose the zero dispersion wavelength(s) (ZDW), to tailor the FWM phase-matching properties [31] and to design fibers approaching endlessly single-mode behavior [32].

The FWM phase-matching properties are determined by the fundamental mode propagation constant, given in terms of the effective refractive index n_{eff} by $k(\omega) = n_{eff}(\omega)\omega/c$. We adopt a step-index model, where the core has radius r , its index is that of fused silica $n_s(\omega)$, and the cladding index is calculated as $n_{clad}(\omega) = f + (1 - f)n_s(\omega)$, where f is the air-filling fraction. This fiber dispersion model has been shown to be accurate for f from 0.1 to 0.9 according to Ref. [33]. In the context of our work, this model permits a straightforward exploration of the spectral entanglement properties in $\{r, f\}$ parameter space.

The structure of the SFWM two-photon state, in the degenerate-pump, co-polarized case (for which $\gamma_1 = \gamma_2 = \gamma$) is illustrated in Fig. 1, for a specific fiber with $r = 0.67\mu\text{m}$, $f = 0.52$ and length $L = 30\text{cm}$. Fig. 1(a) shows the pump envelope function plotted as a function of ω_s and ω_i (see Eq.(7)) where we have assumed that the pump is centered at 723nm, has a bandwidth of 1nm, the incident power is 5W and $\gamma = 70\text{km}^{-1}\text{W}^{-1}$. Fig. 1(b) shows the phasematching function (see Eq.(8)) for this choice of parameters. Note that the phasematched region forms a strip on $\{\omega_s, \omega_i\}$ space, oriented at an angle $\theta_{si} = -\arctan(\tau_s/\tau_i) = -55^\circ$ with respect to the ω_s axis. Fig. 1(c) shows the resulting joint spectral intensity $|F_{lin}(\omega_s, \omega_i)|^2$ (see Eq.(6)). It is apparent from Fig. 1 that the properties of the two photon state are determined by the i) relative orientations and ii) widths of the strips representing the phasematching and pump envelope functions. In this paper we explore how the interplay of the various design parameters can lead to two-photon states with engineered spectral entanglement properties.

A plot of the perfect phase-matching contour ($\Delta k(\omega_p, \omega_s, 2\omega_p - \omega_s) = 0$) for degenerate pumps versus ω_s and ω_p gives for each pump frequency the expected signal and idler central frequencies ω_s^0 and ω_i^0 . Such a phase-matching contour is illustrated in Fig. 2 for $r = 0.616\mu\text{m}$ and $f = 0.6$, with pump power 30W and $\gamma = 70\text{km}^{-1}\text{W}^{-1}$, where the generated frequencies are expressed as detunings from the pump frequency $\Delta_{s,i} = \omega_{s,i} - \omega_p$. Note that energy conservation implies that $\Delta_s = -\Delta_i$. PCFs often have two ZDWs, where one can be as low as 500 nm (in comparison with 1270 nm for bulk silica). The phase-matching contours take the form of closed loops, with inner branches near the pump frequency and outer branches that can be hundreds of nanometers from the pump wavelength. Note that four wave mixing relying on outer-branch phasematching has been observed in previous work, in the context of classical non-linear optics [15].

For this specific fiber geometry, a continuous pump wavelength range of approximately 453 nm exists, in which parametric generation can be observed, almost completely contained between the two ZDWs ($\lambda_{zd1} = 0.668\mu\text{m}$ and $\lambda_{zd2} = 1.132\mu\text{m}$). The power-induced phase modulation terms in Δk split the trivial $\Delta_s = \Delta_i = 0$ branch, leading to frequency-distinct inner-branch signal/idler frequencies close to the pump (used for SFWM in [13]), whereas the outer branch exhibits comparatively little dependence on pump power [15, 16, 17].

In what follows we will concentrate on phase-matching configurations where the signal and idler frequencies are sufficiently removed from the pump frequency, or where the pump is orthogonally polarized to the signal and idler photons, so as to avoid the generation of background photons by spontaneous Raman scattering at the lower-frequency photon of the pair [14].

From Eq. (7) it is clear that the pump envelope function in $\{\omega_s, \omega_i\}$ space has contours of equal amplitude which have negative unit slope in all of $\{\omega_s, \omega_i\}$ space. In contrast, the contours of the phase-matching function $\phi(\omega_s, \omega_i)$ are characterized by a slope in $\{\omega_s, \omega_i\}$ space given by $\theta_{si} = -\arctan(T_s/T_i)$ (with T_μ given according to Eq. (5)). The relationship between the slope $\theta_{\Delta p}$ of the curve at a point in $\{\Delta_{s,i}, \omega_p\}$ space to the resulting phasematching function in $\{\omega_s, \omega_i\}$ space is $\theta_{\Delta p} = 45^\circ - \theta_{si}$. For example, $\theta_{si} = 45^\circ$ corresponds to zero slope on the contour in Fig. 2(a) or $\theta_{\Delta p} = 0$. The colored background in Fig. 2 indicates the slope of the phase-matching contour, or orientation angle, ranging from $\theta_{si} = -90^\circ$ to $\theta_{si} = +90^\circ$, indicated in blue and red respectively.

The type of spectral correlations observed in a SFWM two-photon state is determined in part by the slope θ_{si} of the phase-matching contour. If the phase-matching contour is given by a closed loop (which is true for most fibers, i.e. range of values of $\{r, f\}$, of interest), all phase-matching orientation angles θ_{si} are possible, controlled by the pump frequency. Thus, for certain relative orientations and widths of these two functions, it becomes possible to generate factorable two-photon states. It can be shown that a factorable state is possible if

$$T_s T_i \leq 0. \quad (10)$$

Among those states which fulfil Eq.(10) those exhibiting a phasematching angle of $\theta_{si} = 45^\circ$, or $T_s = -T_i$, are of particular interest. For these states, in the degenerate pumps case, a factorable, symmetric state is guaranteed if

$$2\Gamma\sigma^2|T_s T_i| = 1, \quad (11)$$

where $\Gamma \approx 0.193$. The condition in Eq. (10) constrains the group velocities: either $k^{(1)}(\omega_s) < k^{(1)}(\omega_p) < k^{(1)}(\omega_i)$, or $k^{(1)}(\omega_i) < k^{(1)}(\omega_p) < k^{(1)}(\omega_s)$ must be satisfied. The condition in Eq. (11) constrains the bandwidths. Thus, the region in $\{\omega_s, \omega_i\}$ space in which factorability is possible is bounded by the conditions $T_s = 0$ and $T_i = 0$.

Note that in the case of PDC (in second-order nonlinear crystals), it is in general terms challenging to obey Eq. (10), for it implies that the pump, say with frequency ω_p , must propagate

at a higher group velocity than one of the generated photons at $\omega_p/2$, which can be interpreted as anomalous group-velocity dispersion. In practice, this can be achieved for certain materials, within a restricted spectral region (usually with PDC in the infrared) in a type-II process, where the polarization of the pump is orthogonal to that of one of the generated photons [18]. In the case of SFWM, because the frequencies (in the degenerate pump regime) will in general obey $\omega_s < \omega_p < \omega_i$ or $\omega_i < \omega_p < \omega_s$, no such anomalous group-velocity dispersion is needed, making it much more straightforward to fulfill the group-velocity matching conditions required for factorable photon pair generation.

Once the dispersion relation for a given fiber geometry has been determined, the next step in designing a factorable photon pair source consists of identifying the pump wavelengths that satisfy the required group-velocity matching, amongst those which also satisfy phase-matching. For this purpose, we refer to the colored background in Fig. 2. Each color corresponds to a different phase-matching orientation angle θ_{si} . In particular, symmetric factorable two-photon states, for which the signal and idler photons have identical spectral widths, are possible if $\theta_{si} = 45^\circ$. In this case symmetric group-velocity matching $2k_p^{(1)} = k_s^{(1)} + k_i^{(1)}$ (or equivalently $T_s = -T_i$) is attained, and the phase-matching contours are oriented so that its contours have unit slope. The frequency values that fulfill this condition are represented by the dashed line. The pump frequency that permits symmetric factorable states can be determined from the intersection of the phase-matching contour with the group-velocity matching contour.

Similarly, asymmetric factorable two-photon states, for which the signal and idler photons have greatly different spectral widths, are possible if $\theta_{si} = 0^\circ$ or $\theta_{si} = 90^\circ$. This is the case of asymmetric group-velocity matching, for which $k_p^{(1)} = k_s^{(1)}$ or $k_p^{(1)} = k_i^{(1)}$ (or equivalently $T_s = 0$ or $T_i = 0$) is required. In this case the phase-matching contours are oriented parallel to the ω_s or ω_i axes. In addition, Eq. (11) leads to the condition that $T_i \gg 1/\sigma$ (for $T_s = 0$) or $T_s \gg 1/\sigma$ (for $T_i = 0$).

Both symmetric and asymmetric GVM are possible using a number of different configurations. We provide examples of each, exploiting co-polarized as well as cross-polarized SFWM, in the following sections. Note however, that the examples to be shown do not include all possible source designs.

4. Co-polarized fields and degenerate pumps: symmetric factorable states

The synthesis of a symmetric, factorable state is illustrated in Fig. 3 for the same fiber geometry as described above ($r = 0.616\mu\text{m}$ and $f = 0.6$). Figure 3(a) shows the pump envelope function, for a single pump centered at 715 nm with a relatively narrow bandwidth of 0.1nm. Figure 3(b) shows the phase-matching function assuming a fiber length of 25cm, while Fig. 3(c) shows the joint spectral intensity $|F_{lin}(\omega_s, \omega_i)|^2$, exhibiting an essentially factorable character. For comparison, Fig. 3(d) shows the joint spectral intensity obtained by numerical integration of Eq. (2) using the full dispersion (rather than relying on a linear approximation), revealing that this case the linear approximation of the phase-matching condition is in fact an excellent approximation. This source leads to a numerically-obtained state purity defined as $\text{Tr}[\hat{\rho}_s^2]$, where $\hat{\rho}_s$ is the reduced density operator for the signal state, of 0.901. In fact, the departure from ideal purity is mainly due to sidelobes (related to the sinc function) displaced from the central portion of joint spectral intensity shown in Figs. 3(c) and (d). The purity can be increased by filtering out these sidelobes, which in general contain a small fraction of the total flux. Specifically, for the example shown in Fig. 3, two separate narrowband rectangular-profile spectral filters for the signal and idler modes with equal frequency bandwidth of $9.35 \times 10^{11} \text{rad s}^{-1}$ (corresponding to wavelength widths $\Delta\lambda_s \approx 0.1\text{nm}$ and $\Delta\lambda_i \approx 1.2\text{nm}$) increases the purity to 0.981, while reducing the flux by $\lesssim 5\%$.

As pointed out already, one of the advantages of generating factorable, symmetric photon

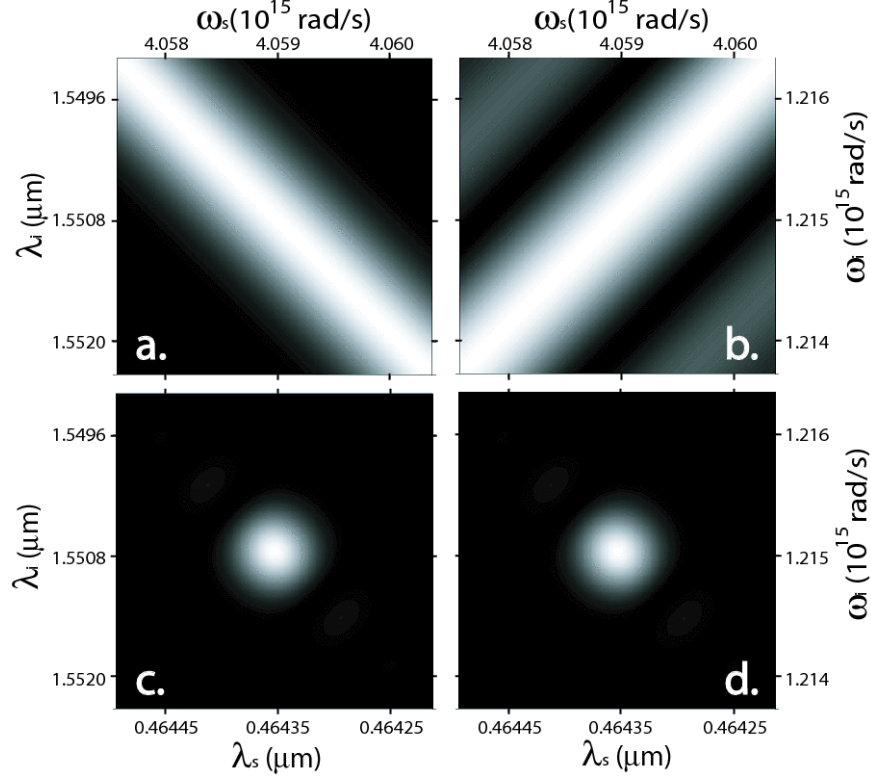


Fig. 3. Joint spectral intensity (JSI) obtained for the fiber geometry assumed for Fig. 2 ($r = 0.616\mu\text{m}$ and $f = 0.6$) where the pump central wavelength ($\lambda_{p0} = 0.7147\mu\text{m}$) is obtained by imposing simultaneous phase-matching and group-velocity matching. We consider a pump bandwidth of 0.1nm and a fiber length of 0.25m . The function values are normalized such that white = 1 and black = 0. (a) Pump envelope function $\alpha(\omega_s, \omega_i)$. (b) Phase-matching function $\phi(v_s, v_i)$. (c) Analytic JSI, obtained with approximation from Eq. (4). (d) JSI obtained by numerical integration of Eq. (2).

pairs through SFWM rather than PDC in a second-order nonlinear crystal, is that it presents greater (but still not arbitrary) choice of the pump, signal and idler frequencies. Thus, for the example shown above, we have chosen the pump so that it is compatible with, say, a Ti:sapphire laser. One of the generated photons is centered at 1551nm , which corresponds to the standard telecommunications band and could be detected with an InGaAs-based avalanche photodetector. The conjugate generated photon is centered at 464nm , which can be detected with a silicon-based avalanche photodiode (though with non-optimal efficiency, since this wavelength is relatively far from the sensitivity peak of such detectors). A natural application for such a source would be the heralding of pure, single photons for transmission over standard optical telecommunication fibers.

5. Co-polarized fields and non-degenerate pumps: symmetric factorable states

The use of non-degenerate pumps represents an additional degree of freedom, not available for PDC in second-order crystals, which can be exploited for state engineering purposes. The two pumps may differ both in terms of their central frequencies (ω_1^0 and ω_2^0) and their bandwidths

(σ_1 and σ_2); in what follows we exploit both of these aspects of non-degeneracy. The orientation of the phase-matching function (see Eqs. (4) and (9)) in $\{\omega_s, \omega_i\}$ space is determined by the angle $\theta_{si} = -\arctan(T_s/T_i)$. Note that the orientation of the phase-matching function depends on σ_1 and σ_2 (through T_s and T_i), while the shape of its profile and its width also depend on σ_1 and σ_2 (through parameter B). A considerable simplification results by imposing the condition $\sigma_1 \ll \sigma_2$. In this case, T_μ reduces to the corresponding degenerate-pump values τ_μ (with $\mu = s, i$). Furthermore, parameter B reduces to $1/(\sigma_1 \tau_p)$, so that the phase-matching function width exhibits no dependence on the broader pump bandwidth (σ_2), while the effective pump envelope function depends only on σ_2 . This de-coupling of σ_1 and σ_2 translates into a more straightforward exploration of possible fiber geometries for the generation of states with specific spectral entanglement properties.

A phase-matching diagram similar to that presented for degenerate pumps (see Fig. 2), may be prepared by maintaining one of the two pump frequencies fixed (in this case pump 2), where it is convenient to express the generated frequencies as detunings from the *mean* pump frequency i.e. $\Delta_{s,i} = \omega_{s,i} - (\omega_1^0 + \omega_2^0)/2$; note that energy conservation implies that $\Delta_s = -\Delta_i$. Figure 4 illustrates the phase-matching properties for a specific non-degenerate geometry, with $r = 0.601 \mu\text{m}$, $f = 0.522$ and $\omega_2^0 = 1.508 \times 10^{15} \text{ rad/sec}$ (that is, $\lambda_2^0 = 2\pi c/\omega_2^0 = 1250 \text{ nm}$). The black solid curve represents the resulting phase-matching contour. The two straight lines represent trivial phase-matching branches (in which the created photons are degenerate with the two pumps), while the loop represents the non-trivial phase-matching branch. Depending on the fiber geometry, the non-trivial branch may become large enough to overlap the trivial branches, or may shrink down to a single point. For the former case, if self-phase modulation becomes appreciable, this contour splits into three distinct loops (rather than two as for degenerate pumps). The colored background represents the orientation angle θ_{si} ranging from -90° in blue to 90° in red.

A factorable, symmetric two-photon state is produced if i) $\theta_{si} = 45^\circ$ which implies $T_s = -T_i$ and ii) the spectral widths of the phase-matching function $\phi(\omega_s, \omega_i)$ and the pump envelope function $\alpha(\omega_s, \omega_i)$ are equal to each other. From Eqs. (5) it is straightforward to show that the first condition is satisfied if the four fields satisfy

$$2k_2^{(1)} - k_s^{(1)} - k_i^{(1)} = -2(k_1^{(1)} - k_2^{(1)})\sigma_1^2/(\sigma_1^2 + \sigma_2^2). \quad (12)$$

This represents a generalization of the equivalent group-velocity matching condition for degenerate pumps (see Eq. 10, and the text which follows). If $\sigma_1 \ll \sigma_2$, the right-hand side of Eq. (12) vanishes, leading to a condition that is identical in form to that obtained for degenerate pumps (where the broader pump now plays the role of the degenerate pump). In Fig. 4, pairs $\{\Delta_s, \omega_{p1}\}$ that satisfy this generalized group-velocity matching condition are represented by a dashed line. Note that the position and shape of this contour in general depend on σ_1 and σ_2 ; however, in the case $\sigma_1 \ll \sigma_2$, the contour becomes decoupled from these bandwidths. Intersection points between the two contours determine the center frequency for pump field 1 that satisfies the requisite group-velocity matching, in addition to phase-matching. The values of r and f are selected so that $\theta_{si} = 45^\circ$ is satisfied *and* so that the broadband pump frequency ω_1^0 takes a certain desired value (in this case, $\lambda_1^0 = 2\pi c/\omega_1^0 = 0.625 \mu\text{m}$). This leads to the generated signal and idler wavelengths 736nm and 960 nm. The fiber length, along with the two bandwidths (subject to $\sigma_1 \ll \sigma_2$) are selected so as to match the widths of the pump envelope and phasematching functions. For the specific geometry shown, these values are $L = 25\text{cm}$, while σ_1 and σ_2 are given in terms of the corresponding FWHM bandwidths: $\Delta\lambda_1 = 1.51 \text{ nm}$ and $\Delta\lambda_2 = 0.12 \text{ nm}$.

An important motivation for exploiting pump non-degeneracy is that it permits SFWM geometries with pumps which are sufficiently distinct from the signal and idler photons, and yet

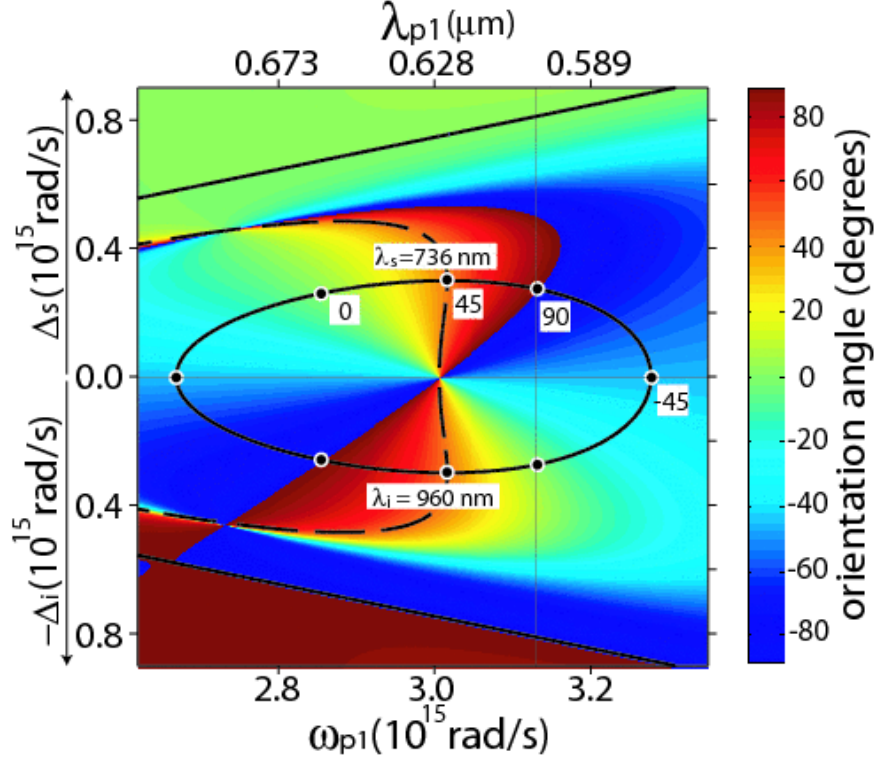


Fig. 4. Black, solid curve: phase-matching ($\Delta k = 0$) contour for SFWM in the non-degenerate pump regime. Colored background: phase-matching orientation angle. Black, dotted line: frequencies that satisfy the group-velocity matching condition (see Eq. (12)). Along the phase-matching contour we have indicated particular angles of orientation of interest.

where the latter are in relative proximity. This is important on the one hand for the suppression of contamination from spontaneous Raman scattering and on the other hand to ensure that both generated photons can be detected with available efficient single-photon detectors. The pump wavelengths were selected so that they can be obtained from a modelocked Cr:Forsterite laser and its second harmonic, while the generated light is within the detection bandwidth of silicon avalanche photo-diodes. Figure 5(a) shows the pump envelope function $\alpha(\omega_s, \omega_i)$. Figure 5(b) shows the phase-matching function $\phi(\omega_s, \omega_i)$ (see Eq.(9)) for which $B = 1.73$. Figure 5(c) shows the resulting joint spectral intensity which exhibits a factorable character, obtained using the linear-dispersion approximation (see Eq. (4)). For comparison, Fig. 5(d) shows the joint spectral intensity obtained by numerical integration of Eq.(2), exhibiting excellent agreement with Fig. 5(c). This source leads to a numerically-obtained state purity of 0.89. As in the case of a factorable symmetric state obtained with degenerate pumps (see Fig. 3), the purity can be increased by filtering out the sidelobes in the joint spectral intensity at small cost in terms of collected flux. Two separate narrowband rectangular-profile spectral filters for the signal and idler modes with equal frequency bandwidth of $12.90 \times 10^{12} \text{ rad s}^{-1}$ (corresponding to wavelength widths $\Delta\lambda_s \approx 3.7 \text{ nm}$ and $\Delta\lambda_i \approx 6.3 \text{ nm}$) increases the purity to 0.98, while reducing the flux by $\lesssim 5.9\%$.

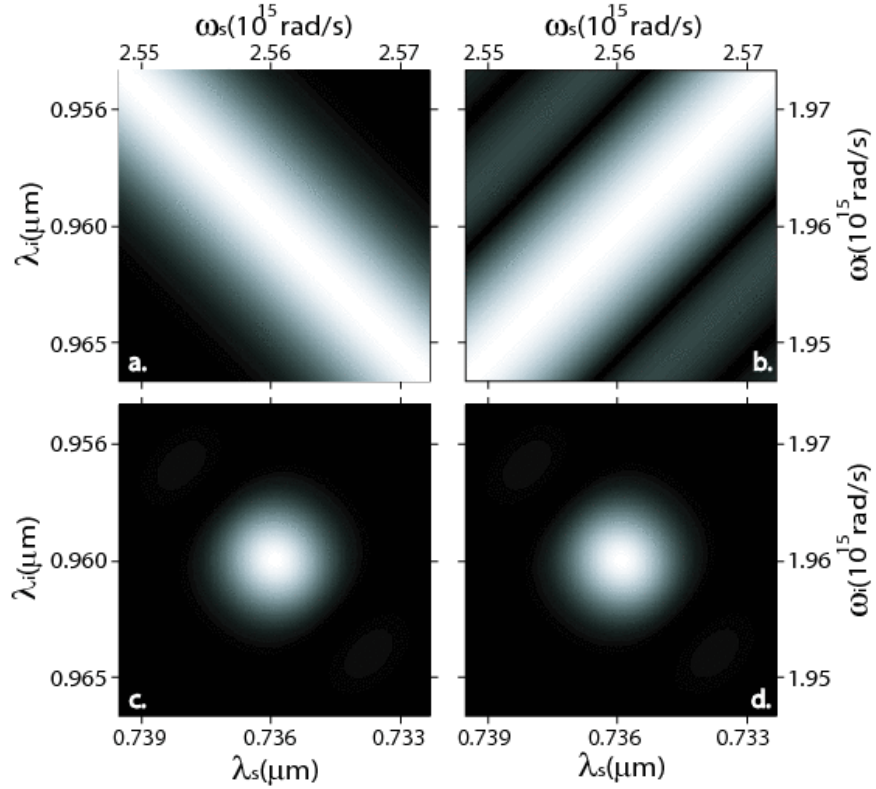


Fig. 5. Joint spectral intensity (JSI) $|F(\omega_s, \omega_i)|^2$ obtained for the fiber geometry assumed for Fig. 4. (a) Pump envelope function $\alpha(\omega_s, \omega_i)$. (b) Phase-matching function $\phi(\omega_s, \omega_i)$. (c) Analytic JSI. (d) JSI obtained by numerical integration of Eq. (2).

6. Cross-polarized fields and degenerate pumps: asymmetric factorable states

Birefringence is an additional degree of freedom that we can use to satisfy the conditions necessary for generating factorable two-photon states. Typical hexagonal pattern PCF can exhibit significant birefringence due to slight asymmetries in the hole pattern or internal stresses in the glass. Birefringence can also be purposefully added to the structure through defects such as two larger holes or elliptical cores. In PCFs, the birefringence typically ranges from $\Delta n \approx 1 \times 10^{-5}$, for normal PCF, to $\Delta n \approx 7 \times 10^{-3}$ [34] for polarization maintaining PCFs.

Conservation of angular momentum restricts the types of FWM processes that can occur in a fiber, with the result that the polarizations of the four fields must appear in pairs in the process [29, 35]. It follows that there are three distinct pair generation processes that can occur in fibers: $xx \rightarrow xx$, $xy \rightarrow xy$, $xx \rightarrow yy$, where x and y can be any two linear orthogonal polarizations. Photon pair generation with frequency separated pumps in the $xy \rightarrow xy$ process was analyzed in 2004 [36] and demonstrated [9] in 2005. In contrast, we limit our discussion to a single pump pulse polarized along one fiber axis (e.g. $xx \rightarrow yy$, $2\omega_p \rightarrow \omega_i + \omega_s$). The first realization of birefringent FWM was a demonstration of this process in regular fibers [37]. It was demonstrated in PCFs in 2006 [38].

Single-photon detectors operating in the visible region of the spectrum are generally less costly and have higher quantum efficiencies and lower noise than single-photon detectors oper-

ating in the near-infrared region. Therefore for some applications it is desirable for both photons from a SFWM pair to be produced in the visible region. This limits the usefulness for these applications of PCFs which have outer-branch solutions far separated from the pump frequency, as shown in Fig. 2(a), as one of the photons is generated in the infrared. On the other hand, the photons should be at least 50 THz from the pump to reduce background from spontaneous Raman scattering. This limits the usefulness of the inner branch solutions, for which the generated photons are typically less than 5 THz from the pump [13]. The benefit of birefringence is that it creates new factorable solutions inside the visible region yet still separated from the pump by more than the Raman bandwidth. Unlike the nondegenerate case, it accomplishes this without the experimental complexity of two pumps. This can be seen by considering the relevant phase-matching equation,

$$\Delta k(\omega_p, \Delta_s) = 2k_x(\omega_p) - k_y(\omega_p + \Delta_s) - k_y(\omega_p - \Delta_s) - \frac{2}{3}\gamma P \quad (13)$$

$$\approx 2k_x(\omega_p) - k_x(\omega_p + \Delta_s) - k_x(\omega_p - \Delta_s) + 2\Delta n \frac{\omega_p}{c} - \frac{2}{3}\gamma P, \quad (14)$$

where the power-induced term is 1/3 of that in the co-polarized case [29]. Some insight can be gained by separating the birefringent contribution to Δk from the individual wavevectors as in Eq. (14). It was experimentally observed in [38] that Δn is approximately independent of frequency and we note that ω_p is relatively constant in comparison to $k_x(\omega_p)$. Consequently, the birefringent contribution to the wavevector mismatch functions much like the power phase-modulation term in Eq. (3), introducing in the $\Delta k = 0$ curve a splitting of the $\Delta_s = 0$ solution (creating the inner branch in Fig. 2). Unlike the power term, the birefringence can create a large splitting and can be either positive or negative.

We begin by extending the step index model reviewed in Section 3 to birefringent fiber. In this extension, each transverse axis of the fiber is modeled as a separate fiber. The axes have the same air-filling fraction parameter f but different core diameters d and $d + \Delta d$, simulating the birefringence [33, 38]. We use this model for all the figures in this section. We also neglect the power term in Eq. (13) since it is typically much smaller than the birefringent contribution. Although this model is accurate only for small birefringence where the fiber asymmetry is small, it allows us to predict universal properties of the SFWM across a broad range of configurations.

In Fig. 6, the phase-matching ($\Delta k(\omega_p, \Delta_{s,i}) = 0$) and group-velocity matching ($T_{s,i} = 0$) curves are plotted for a PCF fiber with ZDWs at 790 nm and 1404 nm, where $d = 1.75 \mu\text{m}$ and $f = 0.43$. Three pairs of curves are plotted for $\Delta d = -0.001, 0, 0.001 \mu\text{m}$, resulting in a birefringence of $\Delta n = -3 \times 10^{-5}, 0, 3 \times 10^{-5}$ (where $\Delta n = n_y - n_x$). The corresponding shift in the ZDW is -0.07, 0, 0.07 nm and $k_x^{(1)} - k_y^{(1)} = -0.5, 0, 0.5 \text{ ps/km}$, respectively. The segments of the $\Delta k = 0$ curve bounded by intersections with the $T_{s,i} = 0$ curve are regions where factorability is possible. For both positive and negative Δn the outer branch intersections remain approximately the same as in the copolarized degenerate case. In addition, negative Δn creates two intersections (Points C and D) in between the two ZDWs. In between these points factorability is possible. Likewise, positive Δn also creates two intersections (Points E and F). However, now it is outside the region bounded by the intersections that factorability is possible. The splitting of the phase-matching ($\Delta k = 0$) solution from the $\Delta_{s,i} = 0$ line in the $\Delta n < 0$ case is similar to that from the power-induced phase modulation term $2\gamma P$ in the phase matching equation Eq. (3), but is an order of magnitude larger. Unlike power-induced inner branch FWM, birefringence allows for phase-matching beyond the Raman peak and is relatively insensitive to pump laser power fluctuations. In contrast, the $\Delta n > 0$ case is qualitatively different from either of these since $2\gamma P$ is always positive in silica. Moreover, it allows for factorable state generation over an unprecedented pump wavelength range, essentially anywhere outside the ZDWs.

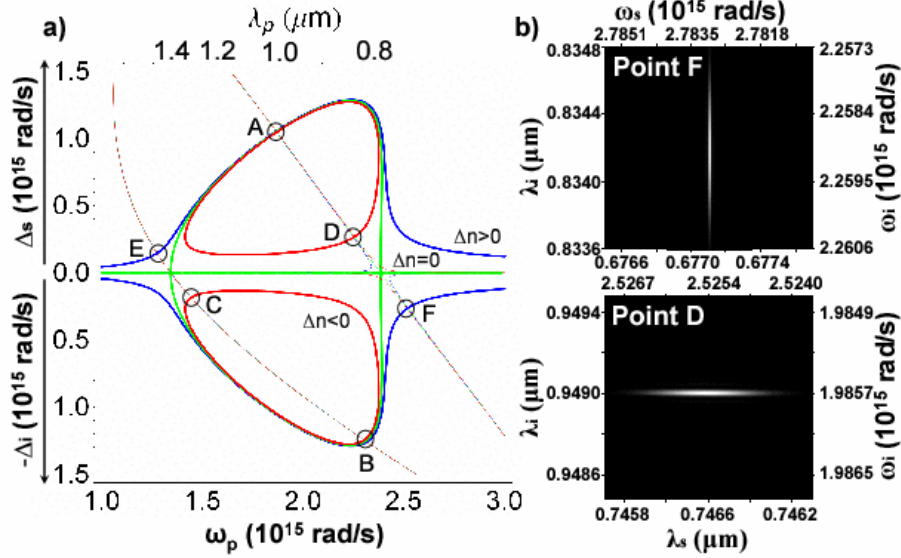


Fig. 6. a) Cross-polarization phase-matching $\Delta k = 0$ (thick) and group-velocity matching $T_{s,i} = 0$ (thin) curves ($f = 0.43$, $d = 1.75 \mu\text{m}$, ZDWs = 790 nm, 1404 nm – similar to NL-1.7-790 from Crystal Fiber). With power $P = 0$, three pairs of curves are plotted with $\Delta d = -0.001, 0, 0.001 \mu\text{m}$, respectively resulting in a birefringence of $\Delta n = -3 \times 10^{-5}, 0, 3 \times 10^{-5}$ (red, green, blue). Points A through F bound regions in which factorability is possible. b) Full dispersion numerical JSIs for the asymmetric states corresponding to points D ($\theta_{si} = 0^\circ$, $\lambda_s = 746.4 \text{ nm}$ and $\lambda_i = 949.0 \text{ nm}$, $\Delta\lambda_p = 0.30 \text{ nm}$, and $L = 30 \text{ m}$) and F ($\theta_{si} = 90^\circ$, $\lambda_s = 677.1 \text{ nm}$, $\lambda_i = 834.2 \text{ nm}$, $\Delta\lambda_p = 0.30 \text{ nm}$, and $L = 30 \text{ m}$).

Figure 6(b) shows the joint spectral intensity in two cases that lead to high degrees of factorability. Factorability corresponds in both cases to the absence of correlation between signal and idler frequencies, as can be seen in the shape of the JSI. In either case, if the idler photon is detected (without spectral filtering), then a nearly pure-state signal photon is heralded. Numerically calculated heralded photon purity for the cases at point F and point D are 0.988 and 0.993, respectively.

In Fig. 7, the intersection of the $\Delta k = 0$ and $T_{s,i} = 0$ curves is plotted as a function of the Δn at 800 nm. Thus for each Δn the figure indicates the pump wavelength λ_p that creates an asymmetric factorable state ($\theta_{si} = 0^\circ$ or $\theta_{si} = 90^\circ$), as well as the center wavelengths λ_s and λ_i of the generated photons. At these points, the pump bandwidth must satisfy condition $T_{s,i} \gg \sigma^{-1}$ but is otherwise arbitrary. The shaded regions indicate the λ_p range in which factorability is possible (including the symmetric state) if the pump bandwidth is set according to Eq. (11).

It has been pointed out in the FWM literature that birefringent FWM has the added benefit of reducing Raman contamination in the signal and idler [39]. Recently this has also been forwarded as a strategy to reduce background for pair-generation [40]. Raman gain g_{Raman} is reduced by as much as an order of magnitude in the axis orthogonal to the strong pump pulse [14]. However, the relevant $\chi^{(3)}$ for birefringent pair production is also reduced by a factor of three compared to co-polarized FWM [29]. Tripling the power P to compensate, Ref. [41] studied the pair-correlation produced by the fiber, $\rho_c(0) = \frac{\langle I_i I_s \rangle}{\langle I_i \rangle \langle I_s \rangle} - 1$, where I is the intensity of signal or idler mode. They found that at the Raman peak, $\rho_c(0)$ was 7 for co-polarized SFWM as compared to 60 for cross-polarized SFWM, indicating that the cross-polarized case can be a

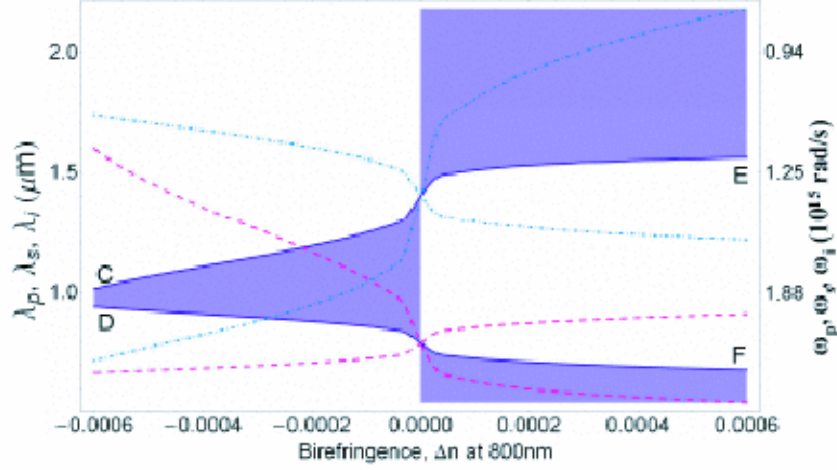


Fig. 7. Points C through F from Fig. 6 are plotted as a function of the birefringence Δn . Thus, the solid dark blue curves give the pump wavelength λ_p of asymmetric factorable solutions. The corresponding idler and signal wavelengths λ_i and λ_s are given by the magenta dashed curves (for points D and F) and light-blue dash-dotted curves (for points C and E). The shaded regions indicate the range in which factorable states can be generated provide the pump bandwidth is matched to the fiber length. The fiber parameters are the same as in Fig. 6.

higher quality photon-pair source.

7. Co-polarized fields: ultra-broadband two-photon states

The flexibility afforded by PCFs in engineering the spectral correlations of photon pairs permits the generation of a wide class of states. For instance, this may be illustrated by considering the generation of quantum states in which the photon pair component has an extraordinarily high degree of frequency anti-correlation[42]. The photons individually have an ultrabroad bandwidth, yet are very tightly anticorrelated in frequency, and highly correlated in time (to the level of a single optical cycle). We have identified conditions for which ultra-broadband two-photon states can be generated in the degenerate pump regime by SFWM. Such ultrabroad states have recently been generated by PDC [43]. As pointed out above, for fiber geometries where the phase-matching diagram occurs in the form of loops (which is true for most cases of interest), it is possible to obtain an arbitrary phase-matching orientation on $\{\omega_s, \omega_i\}$ space. By imposing constraints on higher dispersive orders, it becomes possible to generate states with yet different character. In particular, in analogy with the generation of ultra-broadband two-photon states via PDC [43, 44], it can be shown that in the case of SFWM, the bandwidth of the generated light can be made particularly large if the fourth-order $k^{(4)}$ and second order $k^{(2)}$ coefficients vanish simultaneously. In this case, a degenerate pump at the zero-group-velocity-dispersion frequency can lead to a state with a remarkably broad bandwidth (hundreds of nanometers), even for a nearly monochromatic pump. For example, for the PCF described previously with $r = 0.616\mu\text{m}$ and $f = 0.6$, whose phase-matching curve is shown in Fig. 2, pumping at a frequency around 2.82×10^{15} rad/sec (wavelength $\lambda = 668$ nm), where the curve is nearly vertical,

would create photons with a bandwidth of around 2×10^{15} rad/sec ($\Delta\lambda \approx 542$ nm) centered at the pump frequency, depending on the bandwidth of the pump. Previously, light produced by co-polarized pumps was shown to have a bandwidth of 50 nm for CW pumps [45] and 100 nm for pulsed pumps [46]. For cross-polarized CW pumps broadband light of 34 nm was produced [47].

8. Conclusions

We have studied theoretically the spontaneous four wave mixing process in single mode photonic crystal fiber. We have shown that it is possible to design a source so as to yield photon pairs with a broad class of spectrally engineered properties, including factorable and ultra-broadband states. These results are achieved by adjusting the source configuration, including the dispersion (determined by the core radius and air filling fraction) and birefringence of the fiber and the pump frequency or frequencies, bandwidth(s) and polarization(s). The flexibility of the two-photon state engineering arises from the interplay of this large number of control parameters. Factorable signal-idler pair generation allows the production of heralded, high purity single-photon wavepackets, with minimal or no need for spectral filtering.

Factorable state generation is possible if certain group-velocity matching conditions are satisfied, in addition to standard phase-matching. Most fibers (all those for which the phase-matching curve occurs in loops) can achieve all appropriate group-velocity matching conditions by suitable choice of the pump wavelength. This allows one to realize all possible orientations of the joint spectral amplitude of the generated photon pairs. The size of the phase-matching loop is largely determined by the dispersion of the fiber, hence the utility of PCFs. Therefore we find that for specific choices of pump frequency most fiber designs can yield factorable states. This is in contrast with parametric downconversion in second-order nonlinear crystals where such conditions are met at best at isolated frequencies for certain materials, or using more complicated microstructures [4, 23].

An important design consideration is the possible contamination of the frequency sideband modes by photons from spontaneous Raman scattering. This problem can be circumvented in part by cooling the fiber to cryogenic temperatures, thereby suppressing the Raman scattering [10, 48]. We have shown how to circumvent the problem by exploiting a phase-matching configuration where the signal and the idler frequencies are widely separated from the pump frequency (see Fig. 2). If desired, the phase matching in non-birefringent fiber can be engineered to create photon pairs having one photon in the infrared and one photon in the visible. Alternative approaches also discussed in this paper are cross-polarized FWM in birefringent fiber, where the pump and generated photons have orthogonal polarizations, and the use of non-degenerate pumps in a co-polarized regime. We have shown that these approaches lead to sources capable of generating factorable photon pairs where the signal and idler photons are both in the visible, and at the same time are both sufficiently separated from the pump frequency to avoid Raman contamination. We expect these results to be useful in the design of sources for practical implementations of quantum information processing technologies.

Acknowledgments

KGP, and RRR acknowledge CONACYT-México for partial funding through project no. 46492, and ABU acknowledges support from CONACYT-Mexico through grant 46370. IAW, JL and OC were supported by the EPSRC (UK) through the QIP IRC (GR/S82716/01) and through project EP/C013840/1 and by the European Commission under the Integrated Project Qubit Applications (QAP) funded by the IST directorate as Contract Number 015848. HJM and MGR were supported by the National Science Foundation grants numbers ECS-0621723 and PHY-0554842.